PHYSICS OF FLUIDS **25**, 110805 (2013)

A hybrid subgrid-scale model constrained by Reynolds stress

Aman Verma, Noma Park, and Krishnan Mahesh
Department of Aerospace Engineering and Mechanics, University of Minnesota, Minneapolis, Minnesota 55455, USA

(Received 21 August 2012; accepted 24 May 2013; published online 28 August 2013)

A novel constrained formulation for the dynamic subgrid-scale model for large eddy simulation (LES) is proposed. An externally prescribed Reynolds stress is used as the constraint and is imposed in the near-wall region of wall-bounded flows. However, unlike conventional zonal approaches, Reynolds stress is not imposed as the solution, but used as a constraint on the subgrid-scale stress so that the computed Reynolds stress closely matches the prescribed one only in the mean sense. In the absence of an ideal wall model or adequate near-wall resolution, a LES solution at coarse resolution is expected to be erroneous very near the wall while giving reasonable predictions away from the wall. The Reynolds stress constraint is limited to the region where the LES solution is expected to be erroneous. The Germano-identity error is used as an indicator of LES quality such that the Reynolds stress constraint is activated only where the Germano-identity error exceeds a certain threshold. The proposed model is applied to LES of turbulent channel flow at various Reynolds numbers and grid resolutions to obtain significant improvement over the dynamic Smagorinsky model, especially at coarse resolutions. This constrained formulation can be extended to incorporate constraints on the mean of other flow quantities. © *2013 AIP Publishing LLC*. [http://dx.doi.org/10.1063/1.4819145]

I. INTRODUCTION

High Reynolds number flows of practical importance exhibit such a large range of length and time scales that Direct Numerical Simulations (DNS) are rendered impossible for the foreseeable future. Large eddy simulation (LES) is a viable analysis and design tool for complex flows due to advances in massive parallel computers and numerical techniques. LES is essentially an under-resolved turbulence simulation using a model for the unresolved scales to account for the inter-scale interaction between the resolved and the unresolved scales. The success of LES is primarily due to the dominance of the large, geometry dependent, resolved scales in determining important flow dynamics, and statistics.

In LES, the large scales are directly accounted for by the spatially filtered Navier-Stokes equations and the small scales are modeled by the sub-grid scale (SGS) stress. The spatially filtered incompressible Navier-Stokes equations are

$$\frac{\partial \overline{u}_i}{\partial t} + \frac{\partial}{\partial x_j}(\overline{u}_i \overline{u}_j) = -\frac{\partial \overline{p}}{\partial x_i} + \nu \frac{\partial^2 \overline{u}_i}{\partial x_j \partial x_j} - \frac{\partial \tau_{ij}}{\partial x_j}, \qquad \frac{\partial \overline{u}_i}{\partial x_i} = 0, \tag{1}$$

where x_i denotes the spatial coordinates, u_i is the velocity field, p is the pressure, ν is the kinematic viscosity, $\overline{(\cdot)}$ denotes the spatial filter at grid scale Δ, and $\tau_{ij} = \overline{u_i u_j} - \overline{u}_i \overline{u}_j$ is the SGS stress.

It is generally assumed that small scales are more universal and isotropic than large scales; eddy viscosity type SGS models are therefore widely used in LES. Unfortunately, however, resolved scale dominance and small-scale isotropy is not always the case such as near the wall in

wall-bounded flows. It is well known that LES with simple eddy viscosity model works poorly under such circumstances.[1–3] This is primarily due to the fact that near the wall, flow structures scale in viscous units. If the near-wall grid is constructed to resolve the large or integral length scales of the flow, these dynamically important near-wall structures remain unresolved. Moreover, near-wall flow structures tend to be anisotropic and simple SGS models fail to accurately represent the turbulent stress near the wall. It has been estimated that the grid requirement for a wall-resolved LES scales as Re_τ^2,[4] comparable to that for a DNS which scales as $Re_\tau^{9/4}$. In order to overcome this severe resolution requirement, various wall modeling approaches have been suggested and summarized in some excellent review articles.[5,6] One such approach is that of hybridizing Reynolds Averaged Navier-Stokes (RANS) and LES formulations. The present study is motivated by (1) the inherent limitations of the existing hybrid RANS-LES methodologies and (2) the challenges in implementing a robust hybrid RANS-LES framework for complex flows on unstructured grids. A brief review of the limitations of existing hybrid RANS-LES approaches is presented in Sec. I A.

A. Hybrid RANS-LES approaches

The idea of hybridization of RANS and LES methodologies has been investigated by numerous investigators. Schumann[7] had elements of a hybrid approach which used averaged N-S equations as a near-wall model for LES. Speziale[8] proposed SGS models that allow DNS to transition smoothly to a LES to Very LES (VLES) to RANS depending on the computational grid. Along the lines of Speziale's original idea is the Limited Numerical Scales (LNS) of Batten *et al.*[9] and Girimaji's Partially Averaged Navier-Stokes (PANS) model.[10] The most successful approach, however, has been the Detached-Eddy Simulation (DES) by Spalart *et al.*[11] for high Reynolds number complex flows.

The near-wall region of a high Reynolds number wall-bounded flow is more appropriately modeled by RANS than a coarse grid LES whose filter width is greater than the integral scale of the turbulence. DES uses a limiter based on wall distance and local grid spacing to transition from RANS to LES. The idea is to compute the boundary layer ("attached" region) using RANS and use LES away from the wall (in the "separated" region). DES showed moderate success for external flows with massive separation for which it was originally conceived. However, over the years, it has had to evolve to address various issues arising out of different grid and flow situations. Menter and Kuntz[12] found that DES suffered from grid-induced separation where the grid was small enough for the DES limiter to be activated but not small enough for proper LES. This was alleviated in the Delayed DES (DDES) by Spalart *et al.*[13] where dependency on the solution was introduced to prolong the RANS region near the wall and delay separation. DES was also found to have a zonal interface problem when applied to non-separating boundary layer. Nikitin *et al.*[14] showed that when applied to turbulent channel flow, DES results show unnatural change of the slope of the mean velocity at the zonal interface in the log layer (refer to Piomelli and Balaras:[5] p. 366, Figure 10). This log-layer mismatch is explained by the absence (or lack) of resolved scale fluctuation in the RANS zone and resolved by stochastic forcing in the interface region.[15] The Improved Delayed DES (IDDES) due to Shur *et al.*[16] addresses the log-layer mismatch by stimulating instabilities in the zonal interface.

Another hybrid RANS-LES approach is constructed by coupling separate RANS and LES flow solvers which are running on separate domains of a complex geometry. Apart from the huge challenge in the implementation of the coupling of two separate solvers in a parallel computing framework,[17] flow information needs to be exchanged at the RANS-LES interface as boundary conditions. Areas where problems arise are boundary conditions for the RANS turbulence model and those for the LES solver, especially since the RANS region has no temporal fluctuations.[18]

B. An ideal RANS-LES zonal simulation

Since this zonal interface problem might be the main drawback of a hybrid approach, further investigation is performed to determine whether it is an inherent problem or it is caused by curable reasons like modeling/numerical error or switch design. To this end, an ideal zonal simulation of

TABLE I. Grid parameters for turbulent channel flow.

Case	Re_τ	$N_x \times N_y \times N_z$	$L_x \times L_z$	Δx^+	Δz^+	Δy_w^+	$\Delta y_{cen}/\delta$
			LES				
590spec	590	$12 \times 64 \times 16$	$\pi \times \pi/2$	154	58	0.7	0.05
590s	590	$160 \times 64 \times 66$	$2\pi \times \pi$	23.2	28.1	4	0.05
590un	590	$160 \times 66 \times (150, 100)$	$2\pi \times \pi$	23.2	12.4, 18.5	3.5	0.05
1kun	1000	$160 \times 70 \times (150, 100)$	$2\pi \times \pi$	39.3	21, 31.4	4	0.05
2kun	2000	$160 \times 74 \times (150, 100)$	$2\pi \times \pi$	78.5	42, 63	4	0.05
10kun	10 000	$160 \times 90 \times (150, 100)$	$2\pi \times \pi$	393	209, 314	4	0.05
			DNS				
Moser *et al.*[32]	587	$384 \times 257 \times 384$	$2\pi \times \pi$	9.7	4.8	...	0.012
Alamo *et al.*[33]	934	$- \times 385 \times -$	$8\pi \times 3\pi$	11	5.7	...	...
Hoyas and Jimenez[34]	2003	$- \times 633 \times -$	$8\pi \times 3\pi$	12	6.1	...	...

turbulent channel flow is considered, whose governing equation is

$$\frac{\partial u_i}{\partial t} + \frac{\partial u_i u_j}{\partial x_j} = -\frac{\partial p}{\partial x_i} + \frac{1}{Re}\nabla^2 u_i - F_i,$$
$$F_i = \begin{cases} \frac{\partial \tau_{ij}}{\partial x_j}, & y \geq \delta_z \\ \sigma(u_i - U_{\text{RANS}}), & y < \delta_z, \end{cases} \tag{2}$$
$$\frac{\partial u_i}{\partial x_i} = 0,$$

where δ_z is the zonal interface location, U_{RANS} denotes the exact mean velocity from RANS, σ is a forcing coefficient. Reynolds number is $Re_\tau = u_\tau \delta/\nu$ where u_τ denotes friction velocity, δ channel half-width, and ν viscosity. Case 590spec is simulated (described later in Table I) and the details of the pseudo-spectral numerical method used are in Appendix A. The forcing term F_i enforces the RANS solution and attenuates fluctuations for $y < \delta_z$. Therefore, this region corresponds to an ideal RANS region in the zonal simulation. Since there is no forcing in the region $y \geq \delta_z$, this region corresponds to a LES zone. Mean velocity profile and root-mean-square (rms) velocity fluctuations for this simulation is shown in Fig. 1. Though more exaggerated, the predicted mean velocity shows the same jump across the boundary as shown in the DES of Nikitin *et al.*[14] Baggett[19] argues that the velocity jump is unavoidable to balance the rapid jump of Reynolds stress in the log layer. Also, this approach creates false wall-turbulence starting at the zonal interface that has striking similarity with true wall-turbulence (Fig. 1(b)).

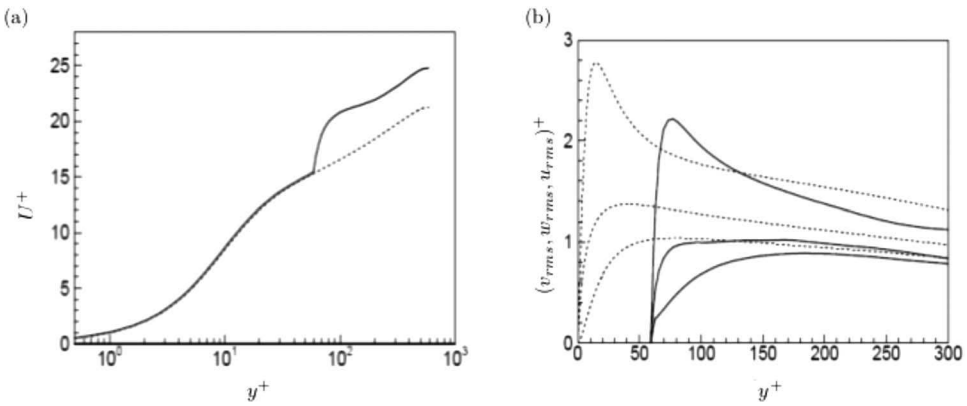

FIG. 1. Mean statistics from turbulent channel flow at $Re_\tau = 590$: (a) mean velocity, (b) rms velocity fluctuations. · · · · · · · · DNS of Moser *et al.*;[32] ——— ideal RANS-LES zonal simulation with $\delta_z^+ = 60$.

C. Proposed hybridization approach

The zonal simulation leads to the conclusion that using a RANS model directly in the near-wall region produces excessive dissipation. A less dissipative "subgrid-scale model" is needed which leads the solution to a target quantity prescribed from external data only in the mean sense. This target quantity may be the wall stress, Reynolds stress, or mean velocity and could be sourced from RANS, DNS, experiments, or even empirical closures/fits. The intention is to perform LES in the whole computational domain. Away from the wall, in general, LES has relaxed grid requirements and simple eddy viscosity models work well. Hence, the external constraint should be imposed in a limited region near the wall where LES is expected to be erroneous.

This paper addresses the "zonal interface issue" inherent in existing hybrid RANS-LES formulations. It proposes a hybrid framework which "seamlessly" couples a desired mean behavior near the wall to a "pure" LES solution away from the wall. Note that the proposed formulation still provides for LES everywhere in the domain. The paper is organized as follows. A hybrid dynamic SGS model constrained by externally prescribed Reynolds stress is formulated in Sec. II. The results of applying the proposed model to turbulent channel flow at various Reynolds numbers and grids, and their discussion is in Sec. III. The applicability of the proposed SGS model as a wall model is studied in Sec. IV. A summary of this work is presented in Sec. V. For completeness, Appendixes A and B provide a short description of the numerical methods and models used.

II. CONSTRAINED DYNAMIC SGS MODEL

The Smagorinsky model[20] for LES is a model for the SGS stress τ_{ij} in terms of the local resolved flow

$$\tau_{ij} - \frac{1}{3}\tau_{kk}\delta_{ij} = -2(C_s\Delta)^2|\overline{S}|\overline{S}_{ij} = -2\nu_t\overline{S}_{ij}, \tag{3}$$

where C_s is a fixed model coefficient, Δ is the filter width, $\overline{S}_{ij}$ is the strain rate tensor, $|\overline{S}| = (2\overline{S}_{ij}\overline{S}_{ij})^{1/2}$ and $\nu_t = (C_s\Delta)^2|\overline{S}|$ are the eddy-viscosity. The Dynamic Smagorinsky model (DSM) due to Germano *et al.*[21] computes a spatially and temporally varying model coefficient C_s. It is based on the Germano identity

$$L_{ij} = T_{ij} - \widehat{\tau}_{ij}, \tag{4}$$

where

$$L_{ij} = \widehat{\overline{u}_i\overline{u}_j} - \widehat{\overline{u}}_i\widehat{\overline{u}}_j, \qquad T_{ij} = \widehat{\overline{u_iu_j}} - \widehat{\overline{u}}_i\widehat{\overline{u}}_j, \quad \text{and} \quad \widehat{\tau}_{ij} = \widehat{\overline{u_iu_j}} - \widehat{\overline{u}_i\overline{u}_j}. \tag{5}$$

Here, $\widehat{(\cdot)}$ denotes test filtering at scale $\widehat{\Delta}$ and is usually taken to be $\widehat{\Delta} = 2\Delta$. L_{ij} is the stress due to scales intermediate between Δ and 2Δ and can be computed directly from the resolved field. T_{ij} is analogous to τ_{ij} and is the corresponding SGS stress at the test filter scale

$$T_{ij} - \frac{1}{3}T_{kk}\delta_{ij} = -2(C_s\widehat{\Delta})^2|\widehat{\overline{S}}|\widehat{\overline{S}}_{ij}. \tag{6}$$

The dynamic procedure to obtain the SGS model coefficient C_s attempts to minimize the Germano-identity error (GIE),

$$\begin{aligned}\epsilon_{ij} &= T^d_{ij} - \widehat{\tau}^d_{ij} - L^d_{ij}\\ &= 2(C_s\Delta)^2\left[\widehat{|\overline{S}|\overline{S}_{ij}} - \left(\frac{\widehat{\Delta}}{\Delta}\right)^2|\widehat{\overline{S}}|\widehat{\overline{S}}_{ij}\right] - L^d_{ij}\\ &= (C_s\Delta)^2M_{ij} - L^d_{ij},\end{aligned} \tag{7}$$

where $(\cdot)^d$ denotes the deviatoric parts and $M_{ij} = 2\left[\widehat{|\overline{S}|\overline{S}_{ij}} - \left(\frac{\widehat{\Delta}}{\Delta}\right)^2|\widehat{\overline{S}}|\widehat{\overline{S}}_{ij}\right]$. Since $\epsilon_{ij}(C_s) = 0$ is a tensor equation, C_s is overdetermined. Lilly[22] found the equations to be regularized when minimizing

the GIE in a least-square sense. The cost function to be minimized can be expressed in the form

$$\mathcal{J} = \int_{\Omega} \epsilon_{ij}(\mathbf{x})\epsilon_{ij}(\mathbf{x})d\mathbf{x}, \tag{8}$$

where Ω is the averaging domain. This yields

$$(C_s\Delta)^2 = \frac{(L_{ij}M_{ij})_h}{(M_{ij}M_{ij})_h}, \tag{9}$$

where $(\cdot)_h$ denotes averaging over homogeneous directions for stability.[21]

To enable averaging in complex flows without any homogeneous directions, Meneveau *et al.*[23] developed a Lagrangian version of DSM (LDSM) where C_s is averaged along fluid trajectories. Essentially, LDSM attempts to minimize the pathline average of the local GIE in a least square sense. The objective function to be minimized is given by

$$\mathcal{J} = \int_{\Omega=pathline} \epsilon_{ij}(\mathbf{z})\epsilon_{ij}(\mathbf{z})d\mathbf{z} = \int_{-\infty}^{t} \epsilon_{ij}(\mathbf{z}(t'),t')\epsilon_{ij}(\mathbf{z}(t'),t')W(t-t')dt', \tag{10}$$

where $\mathbf{z}$ is the trajectory of a fluid particle for earlier times $t' < t$ and W is a weighting function to control the relative importance of events near time t, with those at earlier times. Choosing the time weighting function of the form $W(t-t') = T^{-1}e^{-(t-t')/T}$ yields two transport equations for the Lagrangian average of the tensor products $L_{ij}M_{ij}$ and $M_{ij}M_{ij}$ as $\mathcal{I}_{LM}$ and $\mathcal{I}_{MM}$, respectively. Their solution yields

$$(C_s\Delta)^2 = \frac{(L_{ij}M_{ij})_p}{(M_{ij}M_{ij})_p} = \frac{\mathcal{I}_{LM}}{\mathcal{I}_{MM}}, \tag{11}$$

where $(\cdot)_p$ denotes averaging along pathlines and T is a time scale which represents the "memory" of the Lagrangian averaging. Park and Mahesh[24] introduced a dynamic approach to estimate the Lagrangian time scale T based on a correlation of the GIE. Verma and Mahesh[25] developed and applied the model to complex flows on unstructured grids and showed better results over other averaging methods. The large eddy simulations in Sec. III D are performed using DSM with averaging along homogeneous directions (Eq. (9)), and using Lagrangian averaged DSM (Eq. (11)) with dynamic Lagrangian time scale[25] elsewhere in the paper.

An advantage of the dynamic procedure is that various terms can be easily incorporated to form dynamic mixed models.[26] The minimization of an objective function yields the various model coefficients in a mixed model. The construct of a minimization problem also allows the incorporation of constraints. Ghosal *et al.*[27] showed that the averaging and truncation operations on the computed eddy viscosity can be viewed as a constrained minimization of Eq. (7). Shi *et al.*[28] imposed an energy dissipation constraint on the dynamic mixed similarity model. Under the ambit of the dynamic procedure, Eq. (8) can be generalized and the objective function for constrained minimization can be constructed to be of the form

$$\mathcal{J} = \int_{\Omega} \epsilon_{ij}^{\mathcal{L}}\epsilon_{ij}^{\mathcal{L}}d\mathbf{x} + \omega^{\mathcal{C}}\int_{\Omega} \epsilon_{ij}^{\mathcal{C}}\epsilon_{ij}^{\mathcal{C}}d\mathbf{x}, \tag{12}$$

where $\epsilon_{ij}^{\mathcal{L}}$ is a measure of the error in the LES model, $\epsilon_{ij}^{\mathcal{C}}$ is a constraint which is desired to be satisfied, $\omega^{\mathcal{C}}$ is a weighting function, and $\mathcal{L}$ and $\mathcal{C}$ denote LES and constraint, respectively.

For the scope of the present work, only Reynolds stress is considered to be provided as a constraint. More particularly, only a time average of the Reynolds stress needs to be provided and hence it could be sourced from RANS, DNS, experimental statistics, or even empirical closures/fits. A simple and efficient hybrid SGS model is proposed in Subsection II A that incorporates Reynolds stress constraints into the dynamic procedure. This idea was first introduced by Park and Mahesh.[29]

A. Reynolds stress constrained DSM

Performing an ensemble average of the momentum LES equations (Eq. (1)) results in

$$\frac{\partial \langle \overline{u}_i \rangle}{\partial t} + \frac{\partial}{\partial x_j}(\langle \overline{u}_i \rangle \langle \overline{u}_j \rangle) = -\frac{\partial \langle \overline{p} \rangle}{\partial x_i} + \nu \frac{\partial^2 \langle \overline{u}_i \rangle}{\partial x_j \partial x_j} - \frac{\partial}{\partial x_j}(\langle \overline{u}_i \overline{u}_j \rangle - \langle \overline{u}_i \rangle \langle \overline{u}_j \rangle + \langle \tau_{ij} \rangle), \tag{13}$$

where $\langle \cdot \rangle$ denotes an ensemble average, equivalent to $(\cdot)_{t,h}$ = (temporal + spatial averaging in homogeneous directions, if any). Note that $\langle r_{ij} \rangle = \langle \overline{u}_i \overline{u}_j \rangle - \langle \overline{u}_i \rangle \langle \overline{u}_j \rangle$ is the resolved Reynolds stress. Under the Ergodic assumption that $\langle \overline{u}_i \rangle = \langle u_i \rangle$ and $\langle \overline{p} \rangle = \langle p \rangle$, Eq. (13) can be compared with the RANS equations to yield

$$\langle r_{ij} \rangle + \langle \tau_{ij} \rangle = \mathcal{R}_{ij}, \tag{14}$$

where the RANS Reynolds stress $\mathcal{R}_{ij} = \langle u_i u_j \rangle - \langle u_i \rangle \langle u_j \rangle$ is assumed to be available from an external source. Note that this assumption does not strictly hold, if the LES grid is coarser than the RANS grid. Strictly speaking $\langle \overline{u}_i \rangle = \overline{\langle u_i \rangle}$ is always true. The above condition that the ensemble average of the sum of the resolved and SGS stress be equal to the RANS Reynolds stress is desired to be imposed as a constraint.

Using a SGS stress model τ_{ij}^M, the error in Eq. (14) is ensemble-averaged upto the current time t and written instantaneously (for unsteady simulation) as

$$\epsilon_{ij}^{\mathcal{R}} = \langle \overline{u}_i \overline{u}_j \rangle_t - \langle \overline{u}_i \rangle_t \langle \overline{u}_j \rangle_t + \langle \tau_{ij}^M \rangle_t - \mathcal{R}_{ij}, \tag{15}$$

where $\epsilon_{ij}^{\mathcal{R}}$ is the error (and $\mathcal{R}$ denotes RANS), and $\langle (\cdot) \rangle_t = \frac{1}{t} \sum_0^t (\cdot)$ is cumulative, ensemble-averaged up to current time t. When t is sufficiently large, $\epsilon_{ij}^{\mathcal{R}}$ in Eq. (15) represents deviation from Eq. (14) due to SGS modeling error. Thus, the minimization of $\epsilon_{ij}^{\mathcal{R}}$ seems to be a proper RANS constraint. Initially, minimization of $\epsilon_{ij}^{\mathcal{R}}$ forces the current time step's Reynolds stress (resolved+modeled) to closely resemble the target $\mathcal{R}_{ij}$. With such a "close" initial state, the running time averaged Reynolds stress reaches the target fast ($4\delta/u_\tau$ for case 590spec).

Thus, following Eq. (12), the cost function to be minimized can take the form

$$\mathcal{J} = \int_\Omega \epsilon_{ij}^{\mathcal{L}} \epsilon_{ij}^{\mathcal{L}} d\mathbf{x} + \omega^{\mathcal{R}} \int_\Omega \epsilon_{ij}^{\mathcal{R}} \epsilon_{ij}^{\mathcal{R}} d\mathbf{x}, \tag{16}$$

where Ω is the domain, $\epsilon_{ij}^{\mathcal{L}}$ is the LES (Germano-identity) error, and $\omega^{\mathcal{R}}$ is the weight function for RANS constraints. For the sake of brevity, $(C_s\Delta)^2$ is denoted as C_s henceforth. Considering a one-parameter SGS model $\tau_{ij}^M = \tau_{ij}^M(C_s)$, the optimal C_s is given by

$$\delta \mathcal{J}(C_s) = \int_\Omega \frac{\partial}{\partial C_s} \left[\epsilon_{ij}^{\mathcal{L}} \epsilon_{ij}^{\mathcal{L}} + \omega^{\mathcal{R}} \epsilon_{ij}^{\mathcal{R}} \epsilon_{ij}^{\mathcal{R}} \right] \delta C_s d\mathbf{x} = 0, \tag{17}$$

which implies that

$$\frac{\partial}{\partial C_s} \left[\epsilon_{ij}^{\mathcal{L}} \epsilon_{ij}^{\mathcal{L}} + \omega^{\mathcal{R}} \epsilon_{ij}^{\mathcal{R}} \epsilon_{ij}^{\mathcal{R}} \right] = 0. \tag{18}$$

Equation (18) is a general relation that can be used for complex flows and one-parameter SGS models. Averaging along homogeneous directions or pathlines can be incorporated by considering ω to be the averaging domain and by assuming C_s to be constant in ω.

Substituting GIE from Eq. (7) in the first term of the above Eq. (18) leads to

$$\frac{\partial}{\partial C_s} \left[\epsilon_{ij}^{\mathcal{L}} \epsilon_{ij}^{\mathcal{L}} \right] = 2C_s(M_{ij}M_{ij}) - 2(L_{ij}M_{ij}). \tag{19}$$

Clearly, equating Eq. (19) to zero results in the standard DSM (Eqs. (9) and (11)). Next, the RANS Reynolds-stress reconstruction error (Eq. (15)) is considered by substituting the Smagorinsky model

for τ_{ij}^M (Eq. (3)),

$$\begin{aligned}\epsilon_{ij}^{\mathcal{R}} &= \langle r_{ij}\rangle_t - 2\langle C_s|\overline{S}|\overline{S}_{ij}\rangle_t - \mathcal{R}_{ij}\\ &\approx \langle r_{ij}\rangle_t - 2C_s\langle|\overline{S}|\overline{S}_{ij}\rangle_t - \mathcal{R}_{ij}\\ &= \underbrace{\langle r_{ij}\rangle_t - \mathcal{R}_{ij}}_{A_{ij}} - \underbrace{2\langle|\overline{S}|\overline{S}_{ij}\rangle_t}_{B_{ij}} C_s\\ &\equiv A_{ij} - B_{ij}C_s, \end{aligned} \tag{20}$$

where $\langle r_{ij}\rangle_t = \langle\overline{u}_i\overline{u}_j\rangle_t - \langle\overline{u}_i\rangle_t\langle\overline{u}_j\rangle_t$ and C_s is taken out of the $\langle\cdot\rangle_t$ operator. Similar to Eq. (19), the second term of Eq. (18) is

$$\frac{\partial}{\partial C_s}\left[\epsilon_{ij}^{\mathcal{R}}\epsilon_{ij}^{\mathcal{R}}\right] = 2C_sB_{ij}B_{ij} - 2A_{ij}B_{ij}. \tag{21}$$

Inserting Eqs. (19) and (21) in Eq. (18) yields the constrained SGS model coefficient C_s as

$$C_s = \frac{L_{ij}M_{ij} + \omega^{\mathcal{R}}A_{ij}B_{ij}}{M_{ij}M_{ij} + \omega^{\mathcal{R}}B_{ij}B_{ij}}. \tag{22}$$

B. Dynamic determination of $\omega^{\mathcal{R}}$

In principle, the expression for C_s in Eq. (22) is applicable throughout the flow. However, as mentioned earlier, the intention is to apply the external constraint only in a limited region where LES is expected to be erroneous. Figure 2(a) shows that instantaneously, the GIE is high near the wall and infact manifests itself in the form of long correlation times near-wall streaks as shown in Fig. 2(b).

The GIE (Eq. (7)) is proposed as a measure of accuracy of LES utilizing a dynamic Smagorinsky SGS model. In fact, the GIE has been used to compare the performance of different models during LES.[26,30] Figure 3 shows that time-averaged GIE is very high near the wall so that the validity of the Smagorinsky SGS model (Eq. (3)) in this region can be questioned. The external constraint should be active in such regions where the GIE is deemed too high; to be determined by the weight function $\omega^{\mathcal{R}}$. Note that, to transition from RANS to LES, DES uses purely grid parameters such as the wall distance and local grid spacing; its variants incorporate some flow information. The current proposal to use GIE is explicitly dependent on the flow and the underlying SGS model.

The Germano-identity error is normalized by the modeled SGS stress as

$$\mathcal{E} = \epsilon_{ij}^{\mathcal{L}}\epsilon_{ij}^{\mathcal{L}}/\tau_{ij}^M\tau_{ij}^M. \tag{23}$$

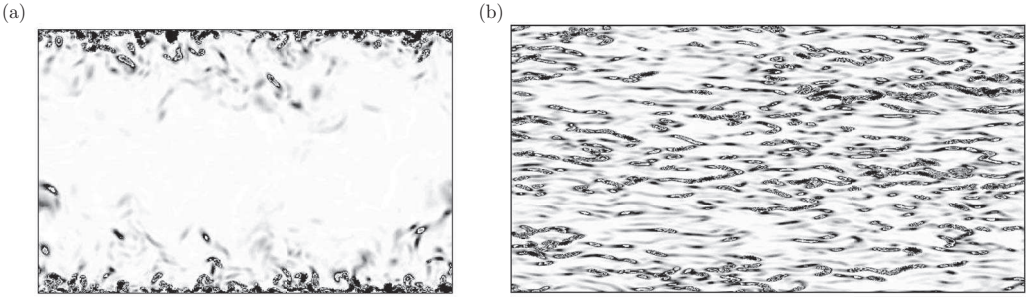

FIG. 2. Instantaneous contours of Germano-identity error $g = \epsilon_{ij}^{\mathcal{L}}\epsilon_{ij}^{\mathcal{L}}/u_\tau^4$ from LES of turbulent channel flow at $Re_\tau = 590$. (a) yz plane, contours vary as $0 \le g \le 3$, (b) xz plane at $y^+ = 12$, contours vary as $0 \le g \le 40$. Reproduced by permission from A. Verma and K. Mahesh, Phys. Fluids **24**, 085101 (2012). Copyright 2012 by American Institute of Physics.

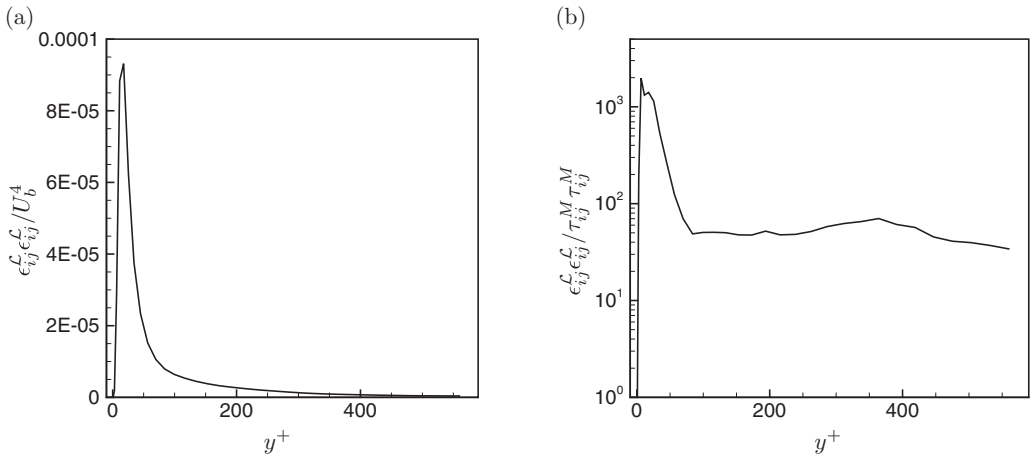

FIG. 3. Turbulent channel flow at $Re_\tau = 590$ – Case 590spec: Germano-identity error normalized by, (a) bulk velocity U_b, (b) modeled subgrid stress.

The weight function $\omega^{\mathcal{R}}$ is then proposed to be of the form

$$\omega^{\mathcal{R}} = C_\omega \max(\mathcal{E} - \mathcal{E}_t, 0), \tag{24}$$

where C_ω is a scaling coefficient and $\mathcal{E}_t$ is the threshold value. Nominally, $C_\omega = 0.1$ and $\mathcal{E}_t = 100$ is chosen to impose the constraints in the near-wall region. Separately, the Eddy Damped Quasi Normal Markovian (EDQNM) analysis of isotropic turbulence also yields $\mathcal{E}_t = 100$. Hence $\omega^{\mathcal{R}} \neq 0$ implies the external constraint is active only in the region where the normalized Germano-identity error $\mathcal{E}$ exceeds a certain threshold $\mathcal{E}_t$. Clearly, $\omega^{\mathcal{R}} = 0$ retrieves the standard DSM (Eq. (9) or Eq. (11)). Sensitivity of the proposed hybrid model to these two parameters is studied in Sec. III C.

Note that such a form for $\omega^{\mathcal{R}}$ is also consistent with Baggett[19] who proposed that the 'blending' function merging the RANS and LES regions of the flow be a function of the resolution and might be parameterized by the ratio of a measure of the filter width and a measure of the turbulent integral dissipation length. It is however, different from a blending function $\beta : 0 \leq \beta \leq 1$ which transitions from pure LES to RANS eddy viscosity.[31]

III. RESULTS

LES is performed for turbulent channel flow at various Reynolds numbers $Re_\tau = u_\tau \delta/\nu$ and grid resolutions as tabulated in Table I. Here u_τ, δ and ν denote the friction velocity, channel half-width, and viscosity, respectively. All cases have uniform spacing in x. Cases 590spec and 590s have uniform spacing in z. The rest have an unstructured grid near the wall in the spanwise direction which allows near-wall spacings (scaling with viscosity) independent of outer region spacings. A slightly finer Δz^+ is used near-wall which is then quickly coarsened to the outer region Δz^+ after 11 rows. Away from the wall in the channel center, the grids are constructed to have almost-isotropic cells; the cell size scales with the outer variables and hence are the same for all Re_τ. Also note that the near-wall Δz is the same; only Δy is varied to achieve the same $\Delta y^+_{wall} \approx 4$. This gridding methodology is used for the unstructured grid cases 590un, 1kun, 2kun, and 10kun. The LES results are compared to DNS whose grid parameters are also included in the table for comparison. Henceforth, DSM denotes Dynamic Smagorinsky Model (Eq. (9) or Eq. (11)) and CDSM denotes Constrained DSM which is the proposed Reynolds stress constrained model (Eq. (22)). The proposed model is validated in Sec. III A, the effect of the imposed constraint is studied in Sec. III B, and the sensitivity to model parameters and numerical methods is discussed in Secs. III C and III D, respectively. The numerical methods employed for the LES and a RANS model to provide the Reynolds stress constraint are briefly described in the Appendix.

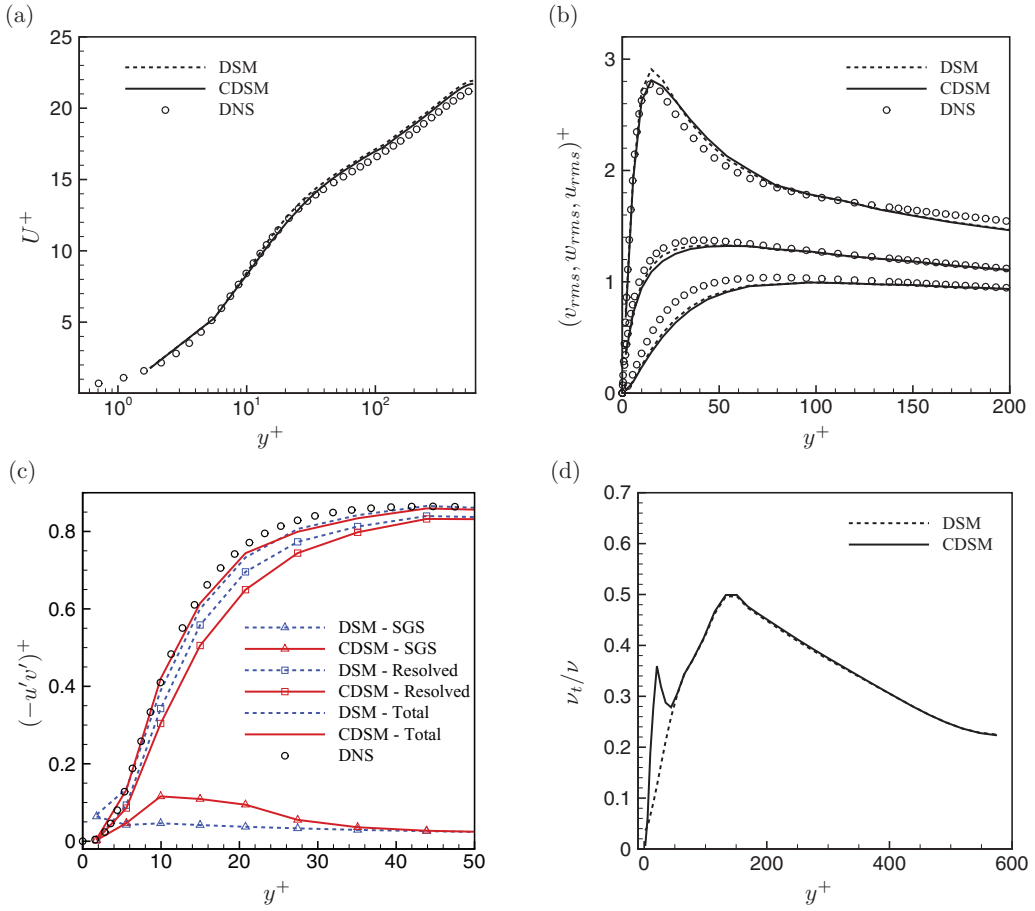

FIG. 4. Mean statistics from turbulent channel flow at $Re_\tau = 590$ – Case 590un: (a) mean velocity, (b) rms velocity fluctuations, (c) Reynolds stress, (d) eddy-viscosity.

A. Validation

Results are shown at $Re_\tau = 590$ and 1000 (cases 590un and 1kun) to provide validation for CDSM as a LES model. An unstructured finite-volume method (Appendix A) is used and the LES terms are Lagrangian averaged (Eq. (11)). Figure 4 shows results from case 590un using the ensemble averaged Reynolds shear stress from the DNS of Moser *et al.*[32] as the constraint. Both DSM and CDSM predict the mean and rms velocity and Reynolds shear stress in good agreement with the DNS of Moser *et al.*[32] In fact, CDSM shows a slight improvement over DSM for mean and rms streamwise velocity. Figure 4(c) shows the resolved, modeled, and total Reynolds stress for DSM and CDSM. For CDSM, the resolved shear stress is slightly lower than DSM near the wall but is compensated by higher SGS stress such that the total shear stress is closer to the DNS constraint than DSM. Eddy viscosity computed due to CDSM is higher near the wall than DSM.

Admittedly, the grid resolution for case 590un is adequate for a reasonably resolved LES. In this limit, CDSM offers marginal improvement over DSM. A coarser grid is used for LES at $Re_\tau = 1000$ and results are shown in Fig. 5 for case 1kun. The mean and rms streamwise velocity and Reynolds shear stress predicted by CDSM is in good agreement with the DNS of Alamo *et al.*[33] The magnitude of peak u_{rms} is better predicted due to reasonable near-wall Δz^+ even though it is shifted due to coarse near-wall Δy^+. Analogous to case 590un, the computed eddy viscosity is higher near the wall using CDSM which increases the modeled SGS stress, compensating for the reduced resolved Reynolds stress such that the total shear stress is closer to the imposed constraint near the wall (Figs. 5(c)–5(d)). This validates the current hybridization procedure to incorporate mean constraints

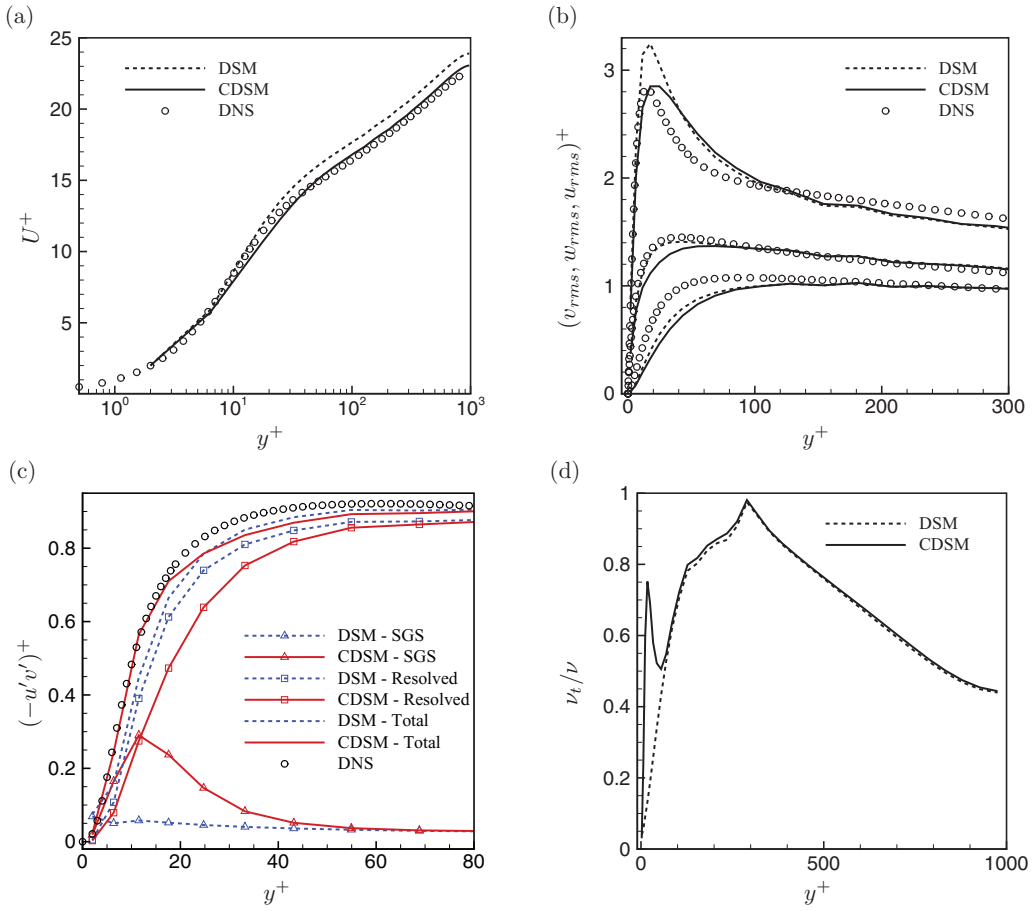

FIG. 5. Mean statistics from turbulent channel flow at $Re_\tau = 1000$ – Case 1kun: (a) mean velocity, (b) rms velocity fluctuations, (c) Reynolds stress, (d) eddy-viscosity.

in an unsteady LES methodology. The mean velocity profile is captured better with CDSM than DSM on coarse grids.

B. Effect of constraint

As seen in Subsection III A, the constraint plays a more significant role on coarser grids when the base SGS stress model is unable to compensate adequately for the reduced resolution (for case 1kun). Hence, the effect of the constraint on the solution is studied at $Re_\tau = 590$ for case 590s which is a coarser grid than that was employed to validate the model in Subsection III A (for case 590un).

Figures 6(a)–6(b) show again that CDSM improves the mean velocity and total Reynolds shear stress prediction compared to DSM. Note that increased Δz^+ resolution near the wall was found to improve the mean velocity prediction (case 590un). For LES on a coarse grid, imposition of a steady constraint in the mean increases the modeled stress and reduces the resolved stress. As a result, L_{ij} and M_{ij} are reduced, resulting in a lower GIE near the wall with CDSM as shown in Fig. 6(c). This indicates that constraining the mean near-wall Reynolds stress to the appropriate value reduces the error inherent in the SGS stress model. Furthermore, Fig. 6(d) shows that only a few points near the wall have the SGS stress normalized GIE greater than the threshold $\mathcal{E}_t$. Hence the constraint is active only at a few points near the wall ($y^+ < 100$) as can be seen by non-trivial values of the weight function $\omega^{\mathcal{R}} > 0$. The near-wall variation of the terms of Eq. (22) are plotted in Fig. 4(e). In the computation of C_s, the term due to the Reynolds stress constraint $\frac{A_{ij}B_{ij}}{B_{ij}B_{ij}}$ is dominant near the wall

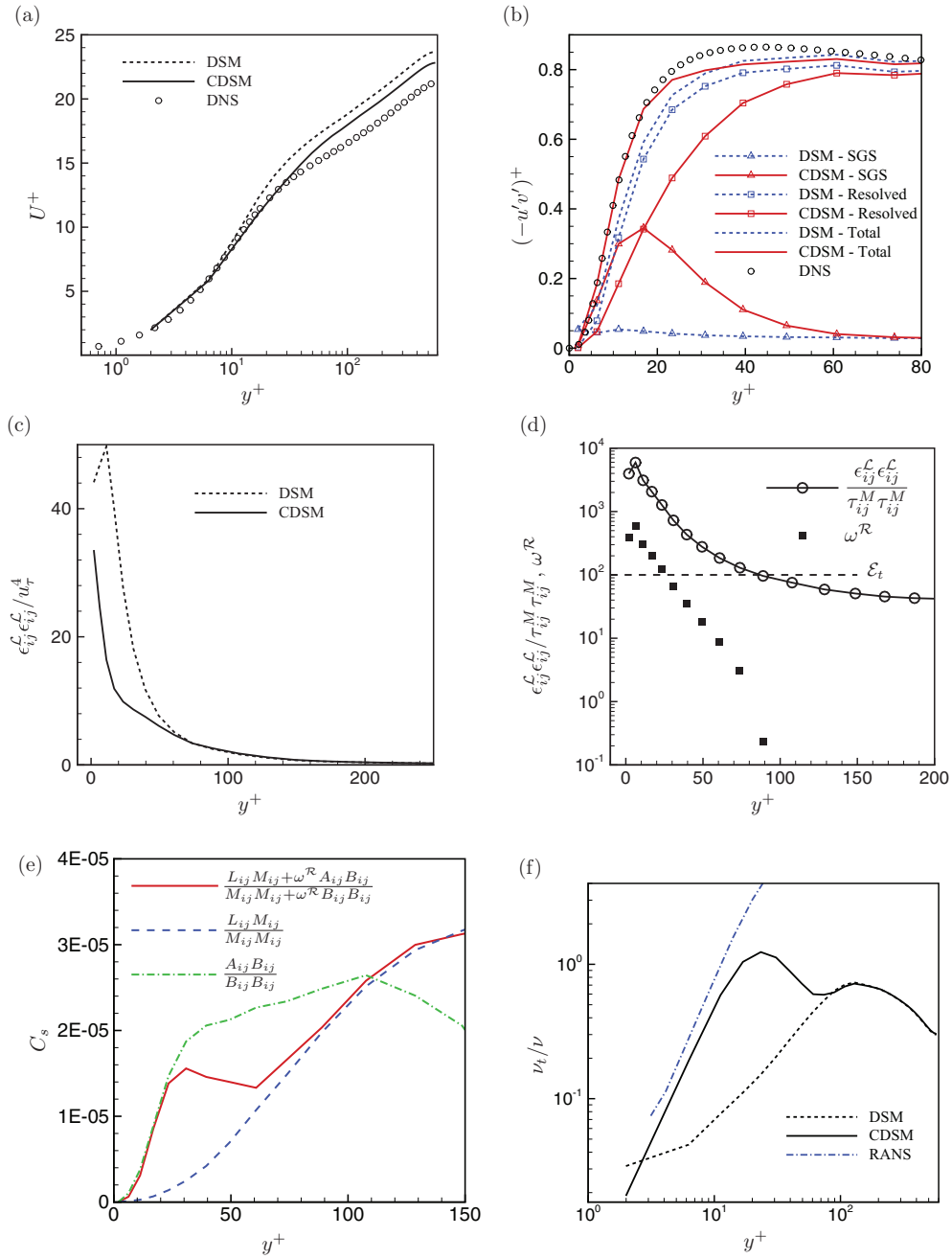

FIG. 6. Mean statistics from turbulent channel flow at $Re_\tau = 590$ – Case 590s: (a) mean velocity, (b) Reynolds stress, (c) Germano-identity error, (d) weight function, (e) model coefficient, (f) eddy-viscosity.

due to high values of $\omega^{\mathcal{R}}$. Away from the wall as $\omega^{\mathcal{R}} \to 0$, $C_s \to \frac{L_{ij}M_{ij}}{M_{ij}M_{ij}}$. Hence the transition and variation of the hybrid C_s given by Eq. (22) (denoted by solid red). Increased C_s results in increased eddy viscosity with CDSM (Fig. 4(f)). The transition of the CDSM ν_t to the DSM ν_t occurs around the same location ($y^+ \sim 80$) where C_s transitions because $\omega^{\mathcal{R}} \to 0$. Also plotted is the RANS eddy viscosity ν_t^+ which is obtained from the non-dimensionalised RANS equation for channel flow

$$(1+\nu_t^+)\frac{du^+}{dy^+} = 1 - \frac{y^+}{Re_\tau},$$

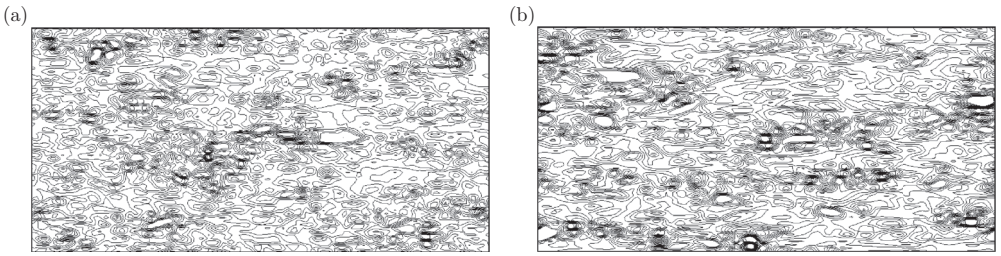

FIG. 7. Instantaneous contours of streamwise vorticity ω_x in the xz plane at $y^+ = 12$ – Case 590s: (a) DSM, (b) CDSM.

where du^+/dy^+ is the gradient of the ensemble averaged streamwise velocity from CDSM. Note that the value of ν_t computed using CDSM approaches and has a similar slope as the RANS ν_t near the wall. Templeton *et al.*[35] provide a relation between the LES and RANS eddy viscosity for channel flow

$$\overline{\nu}_t^{LES} = \overline{\nu}_t^{RANS} + \frac{\langle \overline{u}\overline{v} \rangle}{\langle d\overline{u}/dy \rangle},$$

which also predicts that the mean LES eddy viscosity is always less than the RANS eddy viscosity. Such behavior of the CDSM eddy viscosity near the wall indicates that minimization of the RANS Reynolds-stress reconstruction error $\epsilon_{ij}^{\mathcal{R}}$ (Eq. (15)) could also be construed as a near-wall RANS model.

The effect of the near-wall constraint on the instantaneous flow field is assessed in Fig. 7 which compares streamwise vorticity ω_x in an xz plane near the wall at $y^+ = 12$. Clearly, the small structures are at the same scale for DSM and CDSM. This demonstrates that having an eddy viscosity higher than DSM near the wall did not dissipate away the smaller scales. Different from hybrid RANS/LES methods, Park and Mahesh[24] also reported higher eddy viscosity near the wall and comparable near-wall structures using their control-based DSM which attempts to further minimize the GIE by including the sensitivity of the velocity field to C_s. Hence, the current formulation is indeed behaving as a large eddy simulation all through the domain and may even be successful in predicting higher order statistics near the wall.

C. Sensitivity to $\mathcal{E}_t$ and C_ω

Various numerical experiments have been performed to study the sensitivity of CDSM to the threshold $\mathcal{E}_t$ and scaling coefficient C_ω. Figure 6(d) shows that the normalized GIE has a logarithmic variation near the wall. Hence changing $\mathcal{E}_t$ only by factors may add or remove any significant volume to/from the constrained region. It has indeed been observed that changes of the order of this did not make any apparent difference to the statistics. Note that reducing $\mathcal{E}_t$ to levels which would constrain a significant portion of the domain beyond the near-wall region (e.g., $\mathcal{E}_t = 0$) essentially results in $C_s \sim \frac{A_{ij}B_{ij}}{B_{ij}B_{ij}}$ which is not a desirable SGS stress model for LES (but akin to a RANS model near the wall as shown before). Setting $\mathcal{E}_t$ to low values indeed results in spurious solutions. Increasing $\mathcal{E}_t$ leads to the constraint being active in a smaller region and the solution tends towards DSM. For instance in Fig. 6(d), $\mathcal{E}_t = 100$ results in $\omega^{\mathcal{R}} > 0$ for $y^+ \leq 90$. $\mathcal{E}_t = 1000$ would result in $\omega^{\mathcal{R}} > 0$ for only $y^+ \leq 30$. Unless there is an order of magnitude change in $\mathcal{E}_t$ which would significantly expand or contract the constrained region, it can be said that CDSM is free of sensitivity to a judicious choice of the threshold $\mathcal{E}_t$ limiting it to a small region near the wall. Recall that $\mathcal{E}_t = 100$ is also justified from EDQNM analysis of isotropic turbulence.

Similar to $\mathcal{E}_t$, CDSM is sensitive to only orders of magnitude change in the value of C_ω. Obviously, in the limit $C_\omega \to 0$, CDSM tends to DSM. Increasing C_ω implies a stronger imposition of the constraint over the base SGS stress model. Sensitivity of CDSM to the scaling coefficient C_ω is studied at $Re_\tau = 2000$ and shown in Fig. 8. The coarse near-wall Δz^+ in case 2kun serves to distinguish the performance of CDSM when C_ω is changed by an order of magnitude ($C_\omega = 0.1$

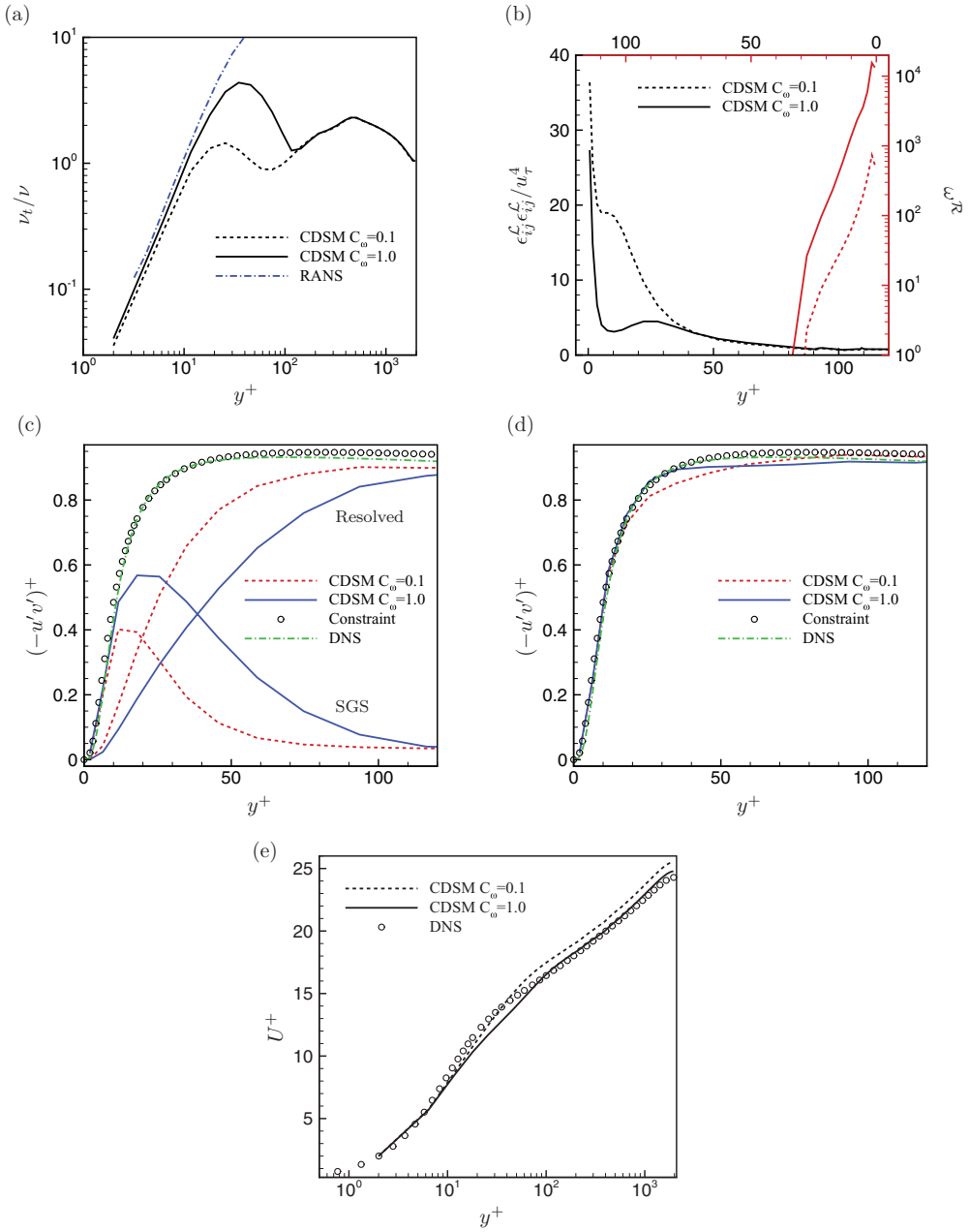

FIG. 8. Mean statistics from turbulent channel flow at $Re_\tau = 2000$ – Case 2kun: (a) eddy-viscosity, (b) Germano-identity error and weight function, (c) resolved and SGS Reynolds stress, (d) total Reynolds stress, (e) mean velocity.

is increased to 1.0). Stronger imposition of the mean Reynolds stress constraint increases the eddy viscosity near the wall, following the RANS eddy viscosity (Fig. 8(a)). As can be expected, Fig. 8(b) shows that the weight function $\omega^{\mathcal{R}}$ is an order of magnitude higher at $C_\omega = 1.0$ than at $C_\omega = 0.1$ and there is a significant drop in GIE near the wall. The increased eddy viscosity leads to higher modeled SGS stress accompanied by a drop in the resolved Reynolds shear stress (Fig. 8(c)). Since $\omega^{\mathcal{R}}$ is a decade higher at $C_\omega = 1.0$, the total Reynolds shear stress is closer to the imposed constraint in the small region around $20 \le y^+ \le 40$ than at $C_\omega = 0.1$ (Fig. 8(d)). The impact on the bulk flow is such that the mean streamwise velocity is slightly closer to the DNS with $C_\omega = 1.0$ (Fig. 8(e)). Hence, CDSM is marginally sensitive to the choice of C_ω.

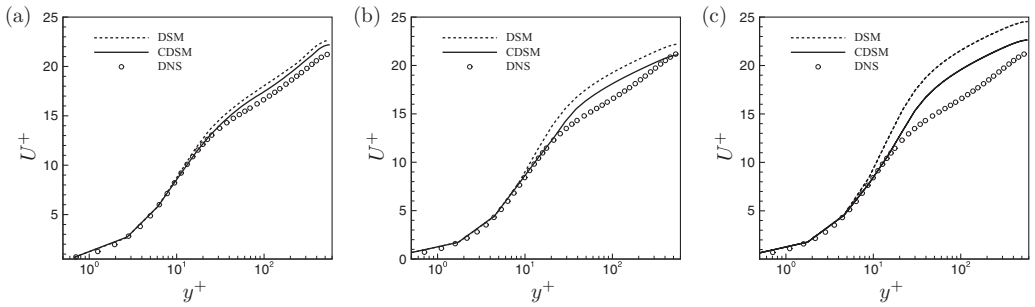

FIG. 9. Mean velocity from turbulent channel flow at $Re_\tau = 590$ (case 590spec) using different numerical methods: (a) pseudo-spectral, (b) finite-difference, (c) unstructured finite-volume.

D. Effect of numerical method

As is true for any simulation methodology, an idea of what constitutes an adequate grid requirement for a reasonable solution is essential, particularly when the intention is to simulate high Reynolds number flows in complex geometries. Apart from the base SGS model, the inherent accuracy of the numerical method plays a major role in the accuracy of results obtained from CDSM on coarse grids. Figure 9 shows mean velocity profiles from using three numerical methods (described in Appendix A): Chebychev pseudo-spectral, structured finite-difference, and unstructured finite-volume method. These results are obtained for case 590spec which has a very coarse near-wall Δz^+ and Δx^+. The Chebychev pseudo-spectral solver produces reasonable results. The log-layer and the outer region are not predicted as accurately by spatially second-order central difference schemes on such a coarse grid. However, CDSM consistently predicts better results than DSM and relatively relaxes the near-wall grid requirement for accurate C_f prediction over DSM.

IV. IMPLICATIONS AS A WALL MODEL

The goal of wall modeling is to relax the near-wall grid scaling with Reynolds number. DES achieves this by operating on a RANS near-wall grid where the wall-parallel spacing is large compared to the boundary-layer thickness ($\Delta_\parallel \gg \delta$) but the wall-normal grid spacing requirement is stricter ($\Delta^+_{\perp,w} \leq 1$). Nikitin *et al.*[14] followed this guideline for their DES of channel flow and showed results with $\Delta_\parallel = 0.1\delta$ and $\Delta y^+_w < 1$. Further savings could be obtained by relaxing the wall-normal grid spacing requirement. When the first off-wall grid point is in the log layer, the filter width is much larger than the local turbulent integral scales. Hence, wall stress models are required to compensate for the SGS modeling errors in this region. Nicoud *et al.*,[36] Templeton *et al.*[35] and various other researchers use walls stress models on coarse grids. Chung and Pullin[37] propose a stretched-vortex SGS model to compute an instantaneous slip velocity at a "virtual wall" which scales with δ.

In this work, LES is performed using no-slip boundary conditions at the wall with a slightly relaxed near-wall grid requirement. Results have been shown with wall parallel coarsening ($\Delta x \geq 0.04\delta$, $\Delta z > 0.02\delta$) and reasonable wall-normal resolution ($\Delta y^+ \sim 4$). For instance, Fig. 8(e) in Sec. III C showed that CDSM predicts the mean velocity for $Re_\tau = 2000$ at such a coarse resolution where DSM is just not expected to perform well. Figure 10 shows that CDSM is able to reasonably predict the mean velocity even when $\Delta z^+_w > 200$ at $Re_\tau = 10\,000$. The reference lines are plotted to allow comparison to the high Re DES of Nikitin *et al.*[14] and LES of Chung and Pullin.[37] The log-law is not well predicted and the Reynolds shear stress is not expected to be resolved; the CDSM constraint compensates by increasing the modeled SGS stress near the wall. At such coarse resolution, there is a log-layer mismatch and CDSM does not work as a proper wall model.

Recall that the target Reynolds stress could be sourced from RANS, DNS, experiments, or empirical closures/fits. For instance, case 590spec uses Reynolds stress from a RANS solution

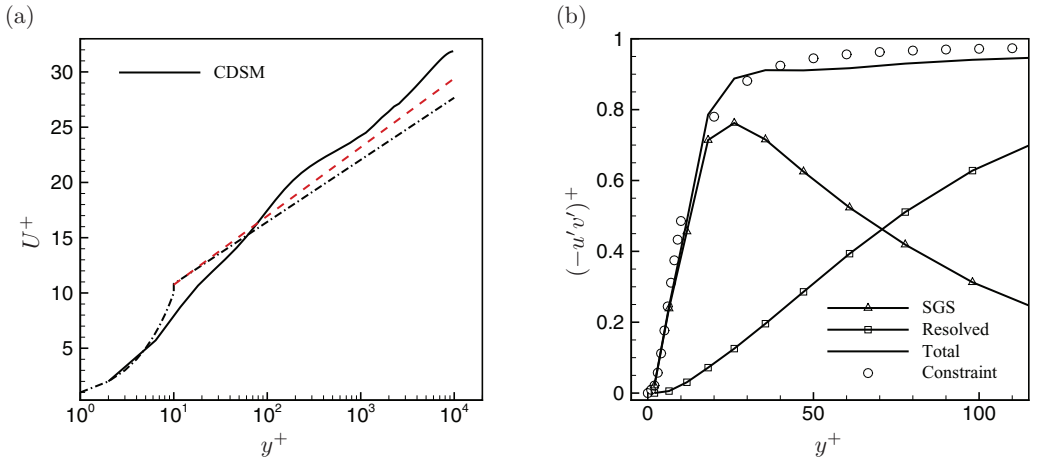

FIG. 10. Mean statistics from turbulent channel flow at $Re_\tau = 10^3$ – Case 10kun: (a) mean velocity; - - - -: $\log(y^+/11)/0.37 + 11$ (Ref. 37); —·—: y^+, $\log(y^+)/0.41 + 5.2$ (Ref. 14), (b) Reynolds stress.

(Appendix B), and cases 590s, 590un, and 1kun use Reynolds stress from DNS. At high Reynolds numbers and complex flows, the target Reynolds stress may not be available *a priori*. A more convenient alternative may be models for Reynolds stress. Such models need only be reasonably accurate in the near-wall region as the constraint is only intended to be applied there. Cases 2kun and 10kun use Reynolds stress obtained using the model described by Perry *et al.*[38] and made available as an online tool. Figure 8(c)–8(d) show that the constraint is in good agreement with DNS near the wall and this is also found to be true for other available DNS data (not shown here). Figure 11 shows that the weight function $\omega^{\mathcal{R}}$ is significant only at some grid points near the wall upto $y \leq 0.07\delta$; this region gets smaller with increasing Re. Hence the Reynolds stress constraint is only active at these points, implying that the target Reynolds stress needs only be accurate in this region near the wall.

The proposed procedure to impose a constraint is general (Eq. (12)) and can in principle, be extended to incorporate constraints other than Reynolds stress. In general, the constraint $\epsilon_{ij}^{\mathcal{C}}$ would need to be expressed as a function of the model coefficient C_s and then the minimization can be carried out either analytically or numerically. For instance, a desired and relatively easily available constraint is the skin friction C_f or wall shear stress τ_w. Then, the velocity U would need to be expressed as an implicit function of C_s and the minimization of $\epsilon_{ij}^{\mathcal{C}}(U(C_s))$ may be carried out in a

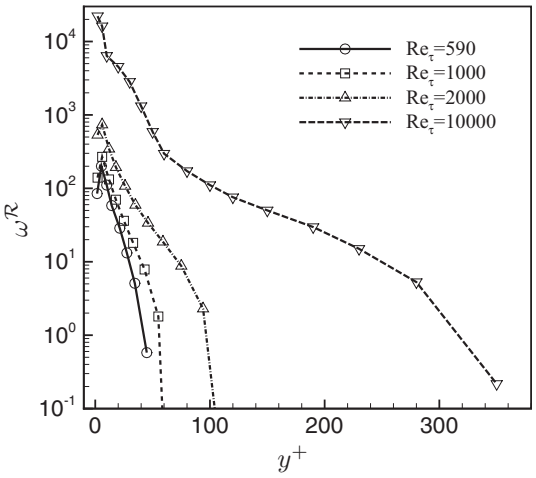

FIG. 11. Comparison of weight function $\omega^{\mathcal{R}}$ from cases 590un, 1kun, 2kun, and 10kun using $C_\omega = 0.1$.

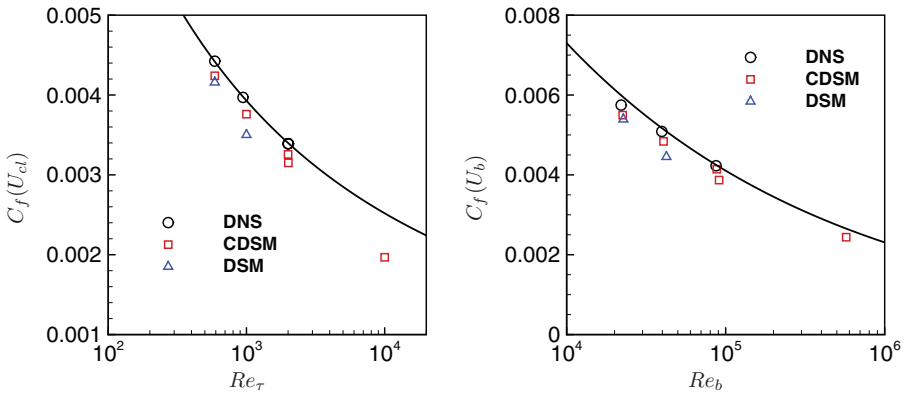

FIG. 12. Skin-friction coefficient C_f from cases 590un, 1kun, 2kun, and 10kun in terms of (a) centerline velocity U_{cl} and Re_τ, ———: extrapolated from the DNS of Moser *et al.*[32] by assuming $U_{cl}^+ = 21.26 + \log(Re_\tau/587)/0.41$ (following Ref. 14), (b) bulk velocity U_b and $Re_b = 2U_b\delta/\nu$, ———: Dean's correlation $C_f = 0.073Re_b^{-1/4}$.[41]

predictor-corrector manner. In fact, such a predictor-corrector approach has been used by Park and Mahesh[24] in their control-based SGS model. However, such "implicit dependence" models would not lend themselves to an algebraic expression for C_s such as Eq. (22). Wikström *et al.*[39] and Fureby *et al.*[40] use a model for the wall eddy viscosity ν_{bc},

$$\nu + \nu_{bc} = \tau_w/(du/dy)_w,$$

where u is given by the law of the wall. Instead of imposing a steady condition like the law of the wall, this expression for the wall shear stress can be imposed in the mean as

$$\langle(\nu + 2C_{s,bc}|S|)\, S_{ij}\rangle_t = \langle\tau_{ij,w}\rangle_t.$$

Analogous to Eq. (15), the constraint can be now be formulated as the error

$$\begin{aligned} \epsilon ij^{\mathcal{R}} &= \langle\tau_{ij}\rangle_t - \langle\nu S_{ij}\rangle_t - \langle C_s|S|S_{ij}\rangle_t \\ &\approx A_{ij} - B_{ij}C_s. \end{aligned}$$

Finally, skin-friction coefficient $C_f = \tau_w/(\frac{1}{2}U^2)$ and wall pressure fluctuations $\sigma(p)/\tau_w$ are plotted in Figs. 12 and 13, respectively. C_f in Fig. 12(a) is based on the centerline velocity U_{cl} and plotted against Re_τ, whereas in Fig. 12(b), it is based on the bulk velocity U_b and bulk Reynolds number $Re_b = 2U_b\delta/\nu$. CDSM is in reasonable agreement with DNS data and empirical fits and it is always better than DSM. Only when the grid is very coarse (case 10kun), CDSM tends to recede

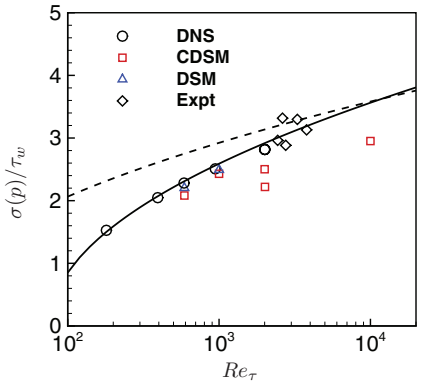

FIG. 13. Wall pressure fluctuations $\sigma(p)/\tau_w$ from cases 590un, 1kun, 2kun, and 10kun. - - - -: $(6.5 + 1.86\log(y^+/333))^{1/2}$ (Ref. 42); ———: $(2.60\log(Re_\tau) - 11.25)^{1/2}$ (Ref. 43); ◇ : experiment of Bull and Thomas.[44]

from the empirical fits. Figure 13 shows that wall pressure fluctuations from CDSM are in good agreement with DNS and the empirical fit at $Re_\tau = 590$ and 1000. However, as the grid coarsens and resolved stress decreases, CDSM predicts decreased resolved $\sigma(p)/\tau_w$ as is expected. Thus, CDSM is a reliable model to perform LES all the way to the wall, better predict skin friction over DSM and also predicts rms wall pressure fluctuations reasonably well.

V. CONCLUSION

DES is a widely used methodology for high Reynolds number external aerodynamics.[45] LES has been used successfully for high Reynolds number separated flows such as in gas turbine combustors[46] and predicting unsteady forces on marine propellers.[47] The strong scaling of the computing cost of LES with Reynolds number is a challenge to LES being applied to attached wall-bounded flows of engineering interest. However, LES for wall-bounded flows offers the advantage of computing fluctuating quantities on the wall such as wall pressure fluctuations and sound.[48]

Nicoud *et al*.[36] note that DES is a suboptimal SGS model because the underlying model is calibrated in the RANS mode. An ideal zonal RANS/LES simulation shows that the zonal interface problem comes from excessive dissipation in the RANS region. The proposed model approaches the mean modeled behavior of RANS through a constraint on what is essentially a SGS model. Primarily, it allows hybridization of the LES methodology with a desired or expected mean target quantity. Currently, external Reynolds stress constraints are incorporated into the Dynamic Smagorinsky model. Second, this target quantity may be imposed in a small region near the wall for wall-bounded flows where SGS modeling errors are expected to be large. Normalized Germano-identity error is used as a measure of SGS modeling errors and hence as a weight for the constraint.

LES is performed for turbulent channel flows at various Reynolds numbers and grid resolutions. CDSM outperforms DSM and this improvement is more apparent as the near-wall grid coarsens. At very coarse resolution, there is a log-layer mismatch and CDSM does not work as a proper wall model. CDSM achieves better predictions than DSM by constraining the total Reynolds stress to an *a priori* imposed target. It has been shown that this target Reynolds stress can be obtained from RANS, DNS, and near-wall models. The model is shown to be marginally sensitive to the scaling coefficient C_ω upto an order of magnitude. Threshold $\mathcal{E}_t$ must be judiciously chosen such that the constraint is imposed only in the near-wall region. Imposition of the near-wall Reynolds stress constraint raises the eddy viscosity and reduces the Germano-identity error.

Finally, this procedure does not force the instantaneous flow to a mean quantity but only constrains the mean behavior. Hence, CDSM predicts unsteady behavior down to the wall and is a reliable tool to predict quantities of engineering interest such as skin friction and wall pressure fluctuations. For future work, CDSM will be applied to complex geometries and separated flows.

ACKNOWLEDGMENTS

This work was supported by the Office of Naval Research under Grant No. N00014-08-1-0433 with Dr. Ki-Han Kim as technical monitor. Computer time was provided by the Arctic Region Supercomputing Center of HPCMP and the Minnesota Supercomputing Institute.

APPENDIX A: NUMERICAL METHOD

1. Unstructured finite-volume

Equation (1) is solved by a numerical method developed by Mahesh *et al*.[46] for incompressible flows on unstructured grids. The algorithm is derived to be robust without numerical dissipation. It is a finite volume method where the Cartesian velocities and pressure are stored at the centroids of the cells, and the face normal velocities are stored independently at the centroids of the faces. A predictor-corrector approach is used. The predicted velocities at the control volume centroids are first obtained and then interpolated to obtain the face normal velocities. The predicted face normal velocity is projected so that the continuity equation in Eq. (1) is discretely satisfied. This yields a

Poisson equation for pressure which is solved iteratively using a multigrid approach. The pressure field is used to update the Cartesian control volume velocities using a least-square formulation. Time advancement is performed using an implicit Crank-Nicolson scheme. The algorithm has been validated for a variety of problems over a range of Reynolds numbers.[46] To improve results on skewed grids, the viscous terms and the pressure Poisson equation are treated differently. The generalized improved deferred correction method by Jang[49] is used to calculate the viscous derivatives and the right-hand side of the pressure Poisson equation.

2. Pseudo-spectral

This numerical method is similar to that used in Kim *et al.*[50] Fourier expansion with 3/2-rule dealiasing for homogeneous (x and z) directions and a Chebychev polynomial expansion is adopted in the wall-normal direction. The governing equations are written in terms of the resolved wall-normal vorticity ($\overline{g} \equiv \partial\overline{u}/\partial z - \partial\overline{w}/\partial x$) and the Laplacian of the resolved wall-normal velocity ($\overline{\phi} \equiv \nabla^2\overline{v}$) to eliminate the pressure, which take the form

$$\begin{aligned} \frac{\partial \nabla^2 \overline{v}}{\partial t} &= h_v + \frac{1}{Re_\tau}\nabla^4 \overline{v}, \\ \frac{\partial \overline{g}}{\partial t} &= h_g + \frac{1}{Re_\tau}\nabla^2 \overline{g}, \\ \nabla \cdot \overline{\mathbf{u}} &= 0, \end{aligned} \tag{A1}$$

where $h_v = -\partial_y(\partial_x H_1 + \partial_z H_3) + (\partial_x^2 + \partial_z^2)H_2$, $h_g = \partial_z H_1 - \partial_x H_3$, and $H_i = -\partial_j(\overline{u}_i\overline{u}_j) - \partial_j \tau_{ij}^M$ ($i = 1, 2, 3$) are nonlinear and SGS terms. Plane-averaged streamwise and spanwise velocities, or wall-parallel velocities at (k_x, k_z) = (0, 0) modes are integrated separately. The flow is driven by a fixed mean pressure gradient, and the governing equation (A1) is naturally normalized in terms of u_τ and δ. h_v and h_g are treated explicitly with the Adams–Bashforth scheme and viscous terms are treated implicitly with the Crank–Nicolson method. A temporal discretization scheme similar to Ref. 51 is used for the implicit treatment of viscous terms. As the test filter of DSM, the sharp cutoff filter is applied to homogeneous directions with $\widehat{\Delta}/\overline{\Delta} = 2$.

3. Structured finite-difference

Equation (1) is solved by a second order fully conservative finite difference scheme in a staggered grid system.[52] A semi-implicit time marching algorithm is used where the diffusion term in the wall normal direction is treated implicitly with the Crank-Nicolson scheme and a third order Runge-Kutta scheme[53] is used for all other terms. The fractional step method[54] is used in order to enforce the divergence free condition. The resulting Poisson equation for the pressure is solved using Fourier Transform in the streamwise and spanwise directions and a tri-diagonal matrix algorithm in the wall normal direction. A three-point Simpson's filter is used as the test filter along the wall parallel directions with $\widehat{\Delta}/\overline{\Delta} = 2$.

APPENDIX B: RANS MODELS

In a practical computation, the Reynolds stress $\mathcal{R}_{ij}$ in A_{ij} (Eq. (20)) could be replaced by RANS model $\mathcal{R}_{ij}^M$. The algebraic eddy viscosity model is given by

$$\mathcal{R}_{ij}^M = -2\nu_T^{\mathcal{R}} \left\langle \overline{S}_{ij} \right\rangle, \tag{B1}$$

where $\nu_T^{\mathcal{R}}$ denotes RANS eddy viscosity. The Spalart-Allmaras model[55] for RANS eddy viscosity ν_T^R is used:

$$\frac{D\tilde{\nu}}{Dt} = c_{b1}\tilde{S}\tilde{\nu} + \frac{1}{\sigma}\left[\nabla \cdot ((\nu + \tilde{\nu})\nabla\tilde{\nu}) + c_{b2}(\nabla\tilde{\nu})^2\right] - c_{w1} f_w \left(\frac{\tilde{\nu}}{d}\right)^2, \tag{B2}$$

where $\nu_T = \tilde{\nu} f_{v1}$, $f_{v1} = \chi^3/(\chi^3 + c_{v1})$, and $\chi = \tilde{\nu}/\nu$. S is either magnitude of vorticity or strain rate. The model is closed with the following coefficients and wall functions:

$$\begin{gathered}
\tilde{S} = S + \frac{\tilde{\nu}}{\kappa^2 d^2} f_{v2},\ f_{v2} = \left(1 + \frac{\chi}{c_{v2}}\right)^{-3}, \\
f_w = g\left(\frac{1+c_{w3}^6}{g^6+c_{w3}^6}\right)^{1/6},\ g = r + c_{w2}(r^6 - r),\ r = \frac{\tilde{\nu}}{\tilde{S}\kappa^2 d^2}, \\
c_{b1} = 0.1355,\ \sigma = \frac{2}{3},\ c_{b2} = 0.622,\ \kappa = 0.41,\ c_{v2} = 5, \\
c_{w1} = \frac{c_{b1}}{\kappa^2} + \frac{1+c_{b2}}{\sigma},\ c_{w2} = 0.3,\ c_{w3} = 2,\ c_{v1} = 7.1.
\end{gathered} \tag{B3}$$

[1] U. Piomelli, Y. Yu, and R. J. Adrian, "Subgrid-scale energy transfer and near-wall turbulence structure," Phys. Fluids **8**, 215 (1996).
[2] J. A. Templeton, M. Wang, and P. Moin, "An efficient wall model for large-eddy simulation based on optimal control theory," Phys. Fluids **18**, 025101 (2006).
[3] N. Park and K. Mahesh, "A velocity-estimation subgrid model constrained by subgrid scale dissipation," J. Comput. Phys. **227**, 4190 (2008).
[4] J. S. Baggett, J. Jiménez, and A. G. Kravchenko, "Resolution requirements in large-eddy simulations of shear flows," in *Annual Research Briefs 1997* (Center for Turbulence Research, Stanford University, 1997), pp. 51–66.
[5] U. Piomelli and E. Balaras, "Wall-layer models for large-eddy simulations," Annu. Rev. Fluid Mech. **34**, 349–374 (2002).
[6] U. Piomelli, "Wall-layer models for large-eddy simulations," Prog. Aerosp. Sci. **44**, 437–446 (2008).
[7] U. Schumann, "Subgrid scale model for finite difference simulations of turbulent flows in plane channels and annuli," J. Comput. Phys. **18**, 376 (1975).
[8] C. G. Speziale, "Turbulence modeling for time-dependent RANS and VLES: A review," AIAA J. **36**, 173–184 (1998).
[9] P. Batten, U. Goldberg, and S. Chakravarthy, "Interfacing statistical turbulence closures with large-eddy simulation," AIAA J. **42**, 485–492 (2004).
[10] S. S. Girimaji, "Partially-averaged Navier-Stokes model for turbulence: A Reynolds-averaged Navier-Stokes to direct numerical simulation bridging method," ASME Trans. J. Appl. Mech. **73**, 413 (2005).
[11] P. R. Spalart, W. H. Jou, M. Strelets, and S. R. Allmaras, "Comments on the feasibility of LES for wings and on a hybrid RANS/LES approach," in *First AFOSR International Conference on DNS/LES*, Ruston, LA (Greyden Press, 1997).
[12] F. R. Menter and M. Kuntz, "Adaptation of eddy-viscosity turbulence models to unsteady separated flow behind vehicles," in *The Aerodynamics of Heavy Vehicles: Trucks, Buses, and Trains*, edited by R. McCallen, F. Browan, and J. Ross (Springer, New York, 2004), pp. 339–352.
[13] P. R. Spalart, S. Deck, M. L. Shur, K. D. Squires, M. Strelets, and A. Travin, "A new version of detached-eddy simulation, resistant to ambiguous grid densities," Theor. Comput. Fluid Dyn. **20**, 181 (2006).
[14] N. V. Nikitin, F. Nicoud, B. Wasistho, K. D. Squires, and P. R. Spalart, "An approach to wall modeling in large-eddy simulations," Phys. Fluids **12**, 1629 (2000).
[15] A. Keating and U. Piomelli, "A dynamic stochastic forcing method as a wall-layer model for large-eddy simulation," J. Turbul. **7**, N12 (2006).
[16] M. L. Shur, P. R. Spalart, M. Strelets, and A. Travin, "A hybrid RANS-LES approach with delayed-DES and wall-modeled LES capabilities," Int. J. Heat Fluid Flow **29**(6), 1638 (2008).
[17] J. U. Schlüter, X. Wu, S. Kim, S. Shankaran, J. J. Alonso, and H. Pitsch, "A framework for coupling Reynolds-averaged with large-eddy simulations for gas turbine applications," J. Fluids Eng. **127**(4), 806 (2005).
[18] J. U. Schlüter, H. Pitsch, and P. Moin, "Large eddy simulation inflow conditions for coupling with Reynolds-averaged flow solvers," AIAA J. **42**(3), 478–484 (2004).
[19] J. S. Baggett, "On the feasibility of merging LES with RANS for the near-wall region of attached turbulent flows," in *Annual Research Briefs* (Center for Turbulence Research, Stanford University, 1998).
[20] J. Smagorinsky, "General circulation experiments with the primitive equations: I. The basic experiment," Mon. Weather Rev. **91**, 99 (1963).
[21] M. Germano, U. Piomelli, P. Moin, and W. Cabot, "A dynamic subgrid-scale eddy viscosity model," Phys. Fluids A **3**, 1760 (1991).
[22] D. K. Lilly, "A proposed modification of the Germano subgrid-scale closure model," Phys. Fluids A **4**, 633 (1992).
[23] C. Meneveau, T. S. Lund, and W. H. Cabot, "A Lagrangian dynamic subgrid-scale model of turbulence," J. Fluid Mech. **319**, 353 (1996).
[24] N. Park and K. Mahesh, "Reduction of the Germano identity error in the dynamic subgrid model," Phys. Fluids **21**, 065106 (2009).
[25] A. Verma and K. Mahesh, "A Lagrangian subgrid-scale model with dynamic estimation of Lagrangian time scale for large eddy simulation of complex flows," Phys. Fluids **24**, 085101 (2012).
[26] R. Anderson and C. Meneveau, "Effects of the similarity model in finite-difference LES of isotropic turbulence using a Lagrangian dynamic mixed model," Flow, Turbul. Combust. **62**(3), 201–225 (1999).
[27] S. Ghosal, T. S. Lund, P. Moin, and K. Akselvoll, "A dynamic localization model for large-eddy simulation of turbulent flows," J. Fluid Mech. **286**, 229 (1995).
[28] Y. Shi, Z. Xiao, and S. Chen, "Constrained subgrid-scale stress model for large eddy simulation," Phys. Fluids **20**, 011701 (2008).

[29] N. Park and K. Mahesh, "A dynamic wall model constrained by external Reynolds stress," in *Proceedings of XXII ICTAM*, Adelaide, Australia (Springer, 2008).
[30] C. Meneveau and J. Katz, "Dynamic testing of subgrid models in large eddy simulation based on Germano identity," Phys. Fluids **11**, 245–247 (1999).
[31] P. Sagaut, *Large Eddy Simulation for Incompressible Flows* (Springer, Berlin, 2002).
[32] R. D. Moser, J. Kim, and N. N. Mansour, "Direct numerical simulation of turbulent channel flow up to $Re_\tau = 590$," Phys. Fluids **11**, 943 (1999).
[33] J. C. del Alamo, J. Jimenez, P. Zandonade, and Robert D. Moser, "Scaling of the energy spectra of turbulent channels," J. Fluid Mech. **500**, 135–144 (2004).
[34] S. Hoyas and J. Jimenez, "Scaling of the velocity fluctuations in turbulent channel flow up to $Re_\tau = 2003$," Phys. Fluids **18**, 011702 (2006).
[35] J. A. Templeton, G. Medic, and G. Kalizin, "An eddy-viscosity based near-wall treatment for coarse grid large-eddy simulation," Phys. Fluids **17**, 105101 (2005).
[36] F. Nicoud, J. S. Baggett, P. Moin, and W. Cabot, "Large eddy simulation wall-modeling based on suboptimal control theory and linear stochastic estimation," Phys. Fluids **13**, 2968 (2001).
[37] D. Chung and D. I. Pullin, "Large-eddy simulation and wall modelling of turbulent channel flow," J. Fluid Mech. **631**, 281–309 (2009).
[38] A. E. Perry, I. Marusic, and M. B. Jones, "On the streamwise evolution of turbulent boundary layers in arbitrary pressure gradients," J. Fluid Mech. **461**, 61–91 (2002).
[39] N. Wikström, U. Svennberg, N. Alin, and C. Fureby, "Large eddy simulation of the flow around an inclined prolate spheroid," J. Turbul. **5**, N29 (2004).
[40] C. Fureby, N. Alin, N. Wikström, S. Menon, N. Svanstedt, and L. Persson, "Large-eddy simulation of high-Reynolds-number wall-bounded flows," AIAA J. **42**, 457–468 (2004).
[41] R. B. Dean, "Reynolds number dependence of skin friction and other bulk flow variables in two-dimensional rectangular duct flow," ASME Trans. J. Fluids Eng. **100**, 215–223 (1978).
[42] T. M. Farabee and M. J. Casarella, "Spectral features of wall presure fluctuations beneath turbulent boundary layers," Phys. Fluids A **3**(10), 2410–2420 (1991).
[43] Z. W. Hu, C. L. Morfey, and N. D. Sandham, "Wall pressure and shear stress spectra from direct simulations of channel flow," AIAA J. **44**(7), 1541–1549 (2006).
[44] M. K. Bull and A. S. W. Thomas, "High frequency wall presure fluctuations in turbulent boundary layers," Phys. Fluids **19**, 597–599 (1976).
[45] P. R. Spalart, "Detached-eddy simulation," Annu. Rev. Fluid Mech. **41**, 181–202 (2009).
[46] K. Mahesh, G. Constantinescu, and P. Moin, "A numerical method for large-eddy simulation in complex geometries," J. Comput. Phys. **197**(1), 215 (2004).
[47] A. Verma, H. Jang, and K. Mahesh, "The effect of an upstream hull with a propeller in reverse rotation," J. Fluid Mech. **704**, 61–88 (2012).
[48] M. Wang and P. Moin, "Dynamic wall modeling for large-eddy simulation of complex turbulent flows," Phys. Fluids **14**(7), 2043 (2002).
[49] H. Jang, "Large Eddy Simulation of crashback in marine propulsors," Ph.D. thesis (University of Minnesota, 2011).
[50] J. Kim, P. Moin, and R. D. Moser, "Turbulence statistics in fully developed channel flow at low Reynolds number," J. Fluid Mech. **177**, 133 (1987).
[51] J. A. Ekaterinaris, "Implicit, high-resolution, compact schemes for gas dynamics and aeroacoustics," J. Comput. Phys. **156**, 272 (1999).
[52] Y. Morinishi, T. S. Lund, O. V. Vasilyev, and P. Moin, "Fully conservative higher order finite difference schemes for incompressible flow," J. Comput. Phys. **143**, 90–124 (1998).
[53] A. A. Wray, "Minimal storage time advancement schemes for spectral methods," Technical Report NASA-Ames Research Center, CA, 1990.
[54] J. K. Dukowicz and A. S. Dvinsky, "Approximation as a high order splitting for the implicit incompressible flow equations," J. Comput. Phys. **102**, 336 (1992).
[55] P. R. Spalart and S. R. Allmaras, "A one-equation turbulence model for aerodynamic flows," La recherche Aérospatiale **1**, 5 (1994).